Large-scale multi-omics analysis suggests specific roles for intragenic cohesin in transcriptional regulation

Jiankang Wang[1,2], Masashige Bando[1], Katsuhiko Shirahige[1,2], Ryuichiro Nakato[1,2,*]

[1]Institute for Quantitative Biosciences, The University of Tokyo; [2]Graduate School of Medicine, The University of Tokyo

*Corresponding author. Tokyo 1130023, Japan. Tel: +81-3-5841-1471; Fax: +81-3-5841-7308; E-mail: rnakato@iqb.u-tokyo.ac.jp

Abstract

Cohesin, an essential protein complex for chromosome segregation, regulates transcription through a variety of mechanisms. It is not a trivial task to genome-widely assign the diverse cohesin functions. Moreover, the context-specific roles of cohesin-mediated interactions, especially on intragenic regions, have not been thoroughly investigated. Here we performed a comprehensive characterization of cohesin binding sites in several human cell types. We integrated epigenomic, transcriptomic and chromatin interaction data with and without transcriptional stimulation, to explore context-specific functions of intragenic cohesin related to gene activation. We identified a new subset of cohesin binding sites, decreased intragenic cohesin sites (DICs), which have a different function from previously known ones. The intron-enriched DICs were negatively correlated with transcriptional regulation: a subgroup of DICs were related to enhancer markers and paused RNA polymerase II, whereas others contributed to chromatin architecture. We implemented machine learning and successfully isolated DICs with distinct genomic features. We observed DICs in various cell types, including cells from cohesinopathy patients. These results suggest a previously unidentified function of cohesin at intragenic regions for transcription regulation.

Keywords: Cohesin, Epigenomics, Transcription regulation, Chromosome structure, Machine learning

Introduction

Cohesin, a ring-shaped chromosome-bound protein complex, is required for holding sister chromatids together during certain phases of the cell cycle[1]. Recent studies suggest that cohesin also has a role in transcription regulation, maintenance of chromosome architecture[2] and DNA repair[3]. The context-specific functions of cohesin have been investigated using chromatin immunoprecipitation followed by sequencing (ChIP-seq) and high-throughput chromosome conformation capture (Hi-C). The early study reported that most cohesin-binding sites overlap with CTCF to function as an insulator[4]. Conversely, a group of cohesin is reported to be CTCF independent and co-bind with tissue-specific transcription factors (TFs) to contribute to transcriptional regulation[5, 6], possibly via the mediation of interactions between enhancers and promoters[7]. Other studies using Hi-C suggested that cohesin and CTCF are essential for forming topologically associated domains (TADs), the evolutionarily conserved chromatin domains that are hundreds of kilobases to several megabases in length[8, 9]. These studies focused on cohesin functions with respect to blocked interactions by insulation, or the formation of enhancer-promoter interactions which implicitly assume the positive regulation of gene expression. In contrast, a recent report showed that transcription elongation within gene bodies causes displacement of cohesin binding from chromatin, leading to disruption of cohesin-mediated chromatin loops[10]. Thus a subset of chromatin loops (either end of which may be located within the intragenic regions) mediated by cohesin is suggested to be negatively correlated with gene activation. Whereas modifications in intragenic regions affect transcription events[11, 12, 13], the function of intragenic cohesin has hardly been discussed.

Mutations in cohesin complex and its loader (NIPBL) are observed in the cohesinopathy Cornelia de Lange syndrome (CdLS), a multisystem developmental disorder[14], and in multiple types of cancers[15, 16]. Our previous study found that the diagnostic phenotype of CdLS is very similar to that of CHOPS syndrome[17], which is caused by missense mutations in AFF4, a core component of the super elongation complex. Given the diverse functions of cohesin with respect to gene expression and chromatin folding, the underlying molecular mechanism responsible for the similarity between CdLS and CHOPS is yet unknown. Noteworthily, the CHOPS-related mutations in super elongation complex are also associated with transcriptional regulation by cohesin, indicating a common pathogenetic mechanism of cohesin in both CHOPS and CdLS. It can be a feasible hypothesis that intragenic cohesin has a distinct role that links the phenotypic similarities between CdLS and CHOPS.

Here, we conducted a large-scale epigenomic analysis to clarify the context-specific functions of cohesin sites, especially those in intragenic regions. To investigate the perturbation of cohesin binding sites by gene activation, we generated RNA sequencing (RNA-seq) and ChIP-seq data for cohesin and

67 several TFs from MCF-7 cells with or without transcription stimulus. We also used many publicly
68 available datasets including Hi-C, ChIP-seq, RNA-seq and chromatin interaction analysis by paired-end
69 tag (ChIA-PET). First, we clarified that a subset of cohesin sites, which we refer to as 'decreased
70 intragenic cohesin sites' (DICs), is distinct from the other groups of cohesin sites. Cohesin bindings on
71 DICs are negatively correlated with transcriptional activation and locus compaction of chromatin. A part
72 of DICs exhibit the high preference for enhancer marks and paused RNA polymerase II, whereas others
73 contribute to chromatin architecture. Second, we performed ChIP-seq and RNA-seq with
74 cohesin-depleted cells and confirmed that cohesin has an active function on DICs. Third, we applied
75 machine learning and captured DICs with distinct epigenomic landscape, which is predictable across cell
76 types. Finally, we conducted plenty of ChIP-seq in other cell types. Importantly, DICs can be observed
77 across multiple cell types, including cells derived from patients with CdLS and CHOPS, in a
78 cell-type-specific manner. The findings from our integrated analysis and machine learning approaches
79 suggest an additional role for cohesin in the regulation of gene expression.
80
81 **Results**
82 *Classification of DICs*
83 MCF-7 cells, when treated with the transcriptional stimulator estradiol[18], is a widely used model for
84 investigating the transcription-dependent perturbation[5]. We prepared ChIP-seq data of cohesin (Rad21),
85 cohesin loader (Mau2), CTCF and several TFs (ER, CBP, P300, AFF4, TAF1) from MCF-7 cells treated
86 with vehicle (control, or Ctrl) or estradiol (E2, 45min). ChIP-seq and RNA-seq data generated in this
87 study and their statistics are summarized in Supplementary Table 1. Other omics data used in this study
88 are listed in Supplementary Tables 2-3. In total, we obtained 76,668 and 89,111 peaks as cohesin
89 binding sites in the E2 and control data, respectively. Next, we examined the stimulation-dependent
90 cohesin sites (Fig. 1a). Although the total number of cohesin peaks decreased after E2 stimulation, the
91 proportion of peaks that increased (9.3%) after stimulation (log-fold change of peak intensity Mvalue[19] >
92 0.5) was larger than the one that decreased (6.2%) (Mvalue < −0.5) (Fig. 1a, bottom). We also found that
93 around 40% (36.3% for E2, 41.2% for control) of cohesin peaks did not overlap with CTCF peaks
94 (Supplementary Fig. 1a). Such 'cohesin-non-CTCF sites' (hereafter, CNCs) overlapped with peaks of the
95 enhancer markers P300 and CBP (Supplementary Fig. 1b), which is consistent with an earlier ChIP-seq
96 study[5]. The cohesin loader Mau2 also preferred enhancer sites. In fact, 88.7% of CNCs with enhancer
97 markers overlapped with Mau2, and Mau2 was localized at enhancer sites with and without cohesin
98 binding (Supplementary Figs. 1c-d). This result implies the role of Mau2 for enhancer activity or for
99 chromatin interaction, which can precede cohesin localization.

100 We classified cohesin sites based on gene annotation information (Supplementary Fig. 1e). We
101 defined 'intragenic cohesin sites' as those located within gene bodies, with the exception of transcription
102 start sites (TSSs), transcription end sites (TESs) and alternative promoters. As a result, 13.8% of cohesin
103 sites were identified as intragenic ones, 19.6% of which had enhancer activities. We did not observe a
104 difference in the proportion of up- or down-regulated cohesin peaks between intergenic and intragenic
105 sites (Fig. 1a, lower panel). To investigate the correlation of cohesin binding and transcription activation,
106 we conducted the ChIP-seq of RNA polymerase II (Pol2), and RNA pol II CTD serine-2 phosphorylation
107 (Pol2ser2) that represents transcription elongation activity[20]. We identified 499 E2-responsive genes for
108 which the Pol2ser2 signal increased after E2 stimulation (Method). We then validated these genes by
109 RNA-seq and confirmed that their expressions were mostly up-regulated by E2 stimulation
110 (Supplementary Fig. 1f). Within the 499 E2-responsive genes, we identified 4,346 intragenic cohesin
111 peaks, 976 (22.4%) of which were decreased after stimulation (Fig. 1b, Supplementary Fig. 1g). Because
112 our main interest is the negative correlation between active transcription and the signal intensity of
113 intragenic cohesin[10], we focused on the intragenic cohesin sites for which the peak intensity decreased
114 after E2 stimulation. Hereafter we refer to these sites as DICs. Among the E2-responsive genes, 53.5%
115 (267/499) contained one or more DICs. We found that almost all (82.8%) DICs were located in intronic
116 regions (Fig. 1c). This result implies a function of DICs on intron, whose mechanism remains
117 unrecognized[21].
118 Next, we investigated the correlation between decreased cohesin binding and the level of chromatin
119 interaction using Hi-C data (GSE99451). Aggregate peak analysis (APA)[22] showed that DICs-centered
120 chromatin interactions were weakened by E2 treatment, whereas no difference was observed for all
121 cohesin sites (Fig. 1d). These results suggested that at least some intragenic cohesin was required for
122 chromatin loop formation, which were disrupted due to the induction of transcription according to
123 previous study[10]. In contrast to the positive regulation of gene expression by CNCs[6], DICs possibly
124 function negatively with respect to gene expression. We then applied DLR (distal-to-local interaction ratio)
125 and ICF (inter-chromosomal fraction of interactions) metrics[10] to represent changes in locus-specific
126 intra- and inter-chromosomal interactions, respectively. The differences (Δ) for DLR or ICF between two
127 Hi-C samples represent chromatin compaction (negative value) or de-compaction (positive value). ΔDLR
128 showed a positive value at DICs (Fig. 1e). In contrast, ΔDLR had a negative peak at all cohesin sites,
129 whereas all enhancers showed no enrichment. Chromatin compaction at all cohesin sites could be
130 explained by more frequent *cis*-regulatory interactions after estrogen stimulation. Conversely, DICs did
131 not show a clear difference as compared with all cohesin sites for ΔICF (Supplementary Fig. 1h). These

results suggested that DICs were involved in intra-chromosome decompaction that created a more open architecture around DICs.

Classification of LC-DICs and HC-DICs

We next investigated the binding pattern of cohesin and other TFs, including the estrogen receptor (ER). We found that DICs could be clearly classified into two categories: HC-DICs (high CTCF binding) and LC-DICs (low CTCF binding), which co-localized with strong and weak CTCF peaks, respectively (Fig. 1f). LC-DICs had a higher probability of co-binding with many TFs as compared with HC-DICs (Figs. 1f-g). This tendency was similar, but not identical, to cohesin peaks in the other regions. For example, cohesin localized with strong CTCF on promoters, where many TFs also bound[6, 23] (Supplementary Fig. 2a). A majority of intergenic cohesin sites (possibly insulator sites or TAD boundaries) did not show TF enrichment (Supplementary Fig. 2b). Moreover, the TFs on LC-DICs (Fig. 1g, Supplementary Fig. 2c, except Mau2 and P300), including 16 publicly available TFs (Supplementary Table 4), were increased after E2 treatment. This suggested that enhancer markers Mau2 and P300 localized to LC-DICs even before stimulation, whereas other TFs, including another enhancer marker CBP, were recruited by E2 stimulation. In addition, the weakened interactions were observed in both LC- and HC-DICs (Supplementary Fig. 2d).

Fig. 1h showed examples of two E2-responsive genes (*MREG* and *PAK4*; see Supplementary Fig. 2e for publicly available TFs). For instance, at the *MREG* locus, there were both HC-DICs, which co-localized with strong CTCF signals but with scarcely any TFs, and LC-DICs, which corresponded with the frequent binding of many TFs yet without strong CTCF signals. Overall, at LC-DICs, the peak intensity of cohesin decreased after E2 stimulation, whereas that of many TFs increased. Consistently, for the E2-activated gene *MREG* (Supplementary Fig. 3a), we could also clearly observe weakened interactions (Fig. 1i) and chromatin decompaction (Supplementary Fig. 3b).

More genomic characteristics were detected by motif analysis (Supplementary Fig. 3c). Not surprisingly, all types of cohesin showed the motifs of CTCF and CTCFL (BORIS). Specifically, LC-DICs were highly enriched for motifs of the forkhead box (FOX) protein family, which is responsible for remodeling chromatin structure[24] and controlling transcription[25]. Of note, FOXA1 is a pioneer factor before ER activation in MCF-7 cells[26]. Meanwhile, HC-DICs showed motifs for transcription repressors including the tumor suppressor gene *HIC1*, implying a possible role for HC-DICs in transcription repression. Taken together, these results highlighted the unique features of LC-DICs and HC-DICs relative to other cohesin sites.

165 *Characterization of LC-DICs as enhancers*

166 The bindings of the enhancer markers CBP and P300 were frequently observed at LC-DICs (Figs.
167 1f-h). We confirmed that a significantly higher percentage of LC-DICs overlapped with CBP binding as
168 compared with other cohesin sites (Fig. 2a, Fisher's exact test). In addition, LC-DICs were also enriched
169 for enhancer markers H3K27ac and H3K4me1 as well as FANTOM5 enhancers[27] (Fig. 2b,
170 Supplementary Fig. 4a; publicly available data). In contrast, HC-DICs were not annotated as enhancers.
171 Moreover, although intergenic cohesin also (including both CTCF-dependent and -independent) in
172 conjunction with many TFs, they were not highly enriched for enhancer markers (Fig. 2a, Supplementary
173 Fig. 4b). This is consistent with the finding that only 18% of intergenic cohesin was co-bound with CBP,
174 which is reasonable because only a subset of intergenic cohesin sites serves as enhancers.

175

176 *Characterization of chromatin loops on DICs*

177 To explore DIC-mediated loops, we investigated what kind of chromatin loci interacted with
178 LC-DICs and HC-DICs. Remarkably, when Pol2-mediated chromatin loops identified by ChIA-PET
179 (GSE33664) were analyzed, the LC-DICs contained multiple Pol2 loops that interacted with the TSS of
180 the host gene, whereas HC-DICs at the *MREG* locus did not have Pol2 loops (Fig. 2b, red arcs). To
181 further investigate this tendency, we also analyzed DIC-anchored loops detected by Hi-C data
182 (GSE99451). Interestingly, this result was in direct contrast to the Hi-C and ChIA-PET Pol2 loops (Fig. 2c,
183 Fisher's exact test). HC-DICs had a significantly lower occurrence probability with respect to
184 Pol2-mediated chromatin loops as compared with LC-DICs and all cohesin sites. In contrast, HC-DICs
185 exhibited a significantly higher occurrence with respect to Hi-C loops. We also compared loops with
186 CTCF ChIA-PET data (GSE39495) and found that over 81% of HC-DICs overlapped with CTCF loops
187 (27% for LC-DICs). This result suggested that LC-DICs were anchored by chromatin loops with Pol2 and
188 other TFs to function as an enhancer in a CTCF-independent manner, whereas HC-DICs were more
189 likely to interact with CTCF to form chromatin loops to participate in chromatin architecture independently
190 of the Pol2 machinery.

191 We then investigated the other anchor sites of the DIC-mediated loops. The other anchor sites of
192 DIC-mediated Hi-C loops also overlapped with cohesin, which also showed decreasing tendency
193 (Supplementary Fig. 5a). As shown in Figs 2d-e, LC-DIC loops (ChIA-PET and Hi-C) mainly interacted
194 with enhancers (40.8%) or promoters (51.2%), which were confirmed by highly enriched active histone
195 markers (Supplementary Fig. 5b). We also observed that only a subset of LC-DIC loops (19.2%)
196 interacted with the promoter of their host genes, suggesting that LC-DICs also contribute to the
197 regulation of distant non-host genes, possibly as intragenic enhancer sites. In contrast, most of the

198 HC-DIC loops did not interact with promoter or enhancer sites (Figs. 2d-e). Instead, over half of these
199 sites interacted with intronic regions (Fig. 2e; example loci are shown in Supplementary Fig. 5c). In
200 summary, these results suggested that LC-DICs participated in transcriptional regulation, whereas
201 HC-DICs were more likely to connect the intronic regions of two genes.
202 We also examined the insulation score (IS) from Hi-C data, for which a lower value indicates more
203 insulated regions, e.g., TAD boundaries. Although the IS profile showed clear valley at all, intergenic and
204 intragenic cohesin sites (Fig. 2f, Supplementary Fig. 5d), it peaked at DICs (Fig. 2f, top left). Interestingly,
205 the IS profile for HC-DICs showed bimodal peaks around small valley, whereas there was neither a peak
206 nor valley at LC-DICs (Fig. 2f, lower right). These results suggested that LC-DICs possibly act as
207 enhancers within TADs and that HC-DICs participate in the formation of boundaries, which is consistent
208 with our loop analysis described above.
209
210 *Assessment of Pol2 stalling on DICs*
211 Pol2 is released from promoter-proximal pausing to transcribe the entire gene body, although it may
212 be temporarily paused by roadblocks within gene bodies[12]. To test whether DICs can function as
213 roadblocks, we investigated the Pol2 enrichment at DICs using our Pol2 and Pol2ser2 ChIP-seq data
214 (Supplementary Fig. 6a). Our Pol2ser2 and public global nuclear run-on sequencing data (GRO-seq,
215 GSE99508) showed that transcription elongation was activated by E2 (Fig. 3a). Moreover, we found that
216 Pol2 peaked at LC-DICs, and its intensity decreased after E2 stimulation (Fig. 3a-b), possibly due to the
217 release of paused Pol2. This tendency toward a decrease in Pol2 binding was statistically significant as
218 compared with the other cohesin sites (Fig. 3c). Importantly, ChIP-seq data treated with E2 for 30min,
219 and public ChIP-seq datasets also showed the decreased Pol2 (Supplementary Figs. 6b-c). Given that
220 bindings of most TFs were increased by E2 stimulation at LC-DICs (Figs. 1g-h), cohesin binding that
221 decreased at LC-DICs was more likely to be accordant with Pol2, rather than TF bindings. In contrast,
222 Pol2ser2 was increased on all DICs due to transcription activation (Fig. 3b, right panel). Pol2ser2 also
223 exhibited peak-like enrichment at LC-DICs, which was increased by E2 stimulation (Figs. 3a-b). This is
224 remarkable given that Pol2 enrichment at LC-DICs decreased significantly after E2 stimulation (Figs.
225 3b-c). In addition, whereas Pol2 binding on TSSs of DIC-host genes did not show any difference after E2
226 stimulation, the intensity of Pol2ser2 on TSSs increased (Supplementary Fig. 6d). These results support
227 the model that Pol2 temporarily stalls within DICs, which function as roadblocks, and then is released by
228 the loss of cohesin.
229
230 *Knockdown analysis of cohesin revealed that cohesin had a function at DICs*

231 Although we observed cohesin binding at DICs that was synchronized with Pol2 binding and was
232 negatively correlated with gene expression, there is still a possibility that cohesin is “passively” localized
233 to DICs and therefore does not have any active role with respect to gene expression. To determine
234 whether cohesin functions in the pausing of Pol2 at LC-DICs, we prepared Pol2 and Pol2ser2 ChIP-seq
235 data in the absence and presence of Rad21-specific siRNA (siRad21) to generate Rad21 knockdown
236 (KD; Supplementary Fig. 6e) and investigate the effect at DICs. Pol2 binding before E2 stimulation was
237 significantly decreased by siRad21 (site 3 vs. 1 in Fig. 3d, KD_Ctrl as compared with WT_Ctrl in Figs.
238 3e-f) and had a similarly low level of binding in E2-treated wild-type cells (site 2 in Fig. 3d, WT_E2 in Figs.
239 3e-f). Thus, KD of cohesin indeed decreased Pol2 on LC-DICs, indicating that cohesin binding on
240 LC-DICs is not passive but is required for Pol2 stalling. Pol2 binding in KD_Ctrl cells was not affected by
241 E2-stimulation (site 4 vs. 3 in Fig. 3d, KD_E2 as compared with KD_Ctrl in Figs. 3e-f), possibly because
242 Pol2 that was paused in WT_Ctrl cells had already been released in KD_Ctrl cells. Importantly, the effect
243 of siRad21 on the Pol2 signal at TSSs of E2-responsive genes was distinct from LC-DICs, in which Pol2
244 binding did not change significantly after E2 stimulation in WT cells (from WT_Ctrl to WT_E2 in Figs. 3d
245 and 3f) but decreased after siRad21 in stimulated cells (from WT_E2 to KD_E2 in Figs. 3d and 3f). These
246 results also supported the model that the loss of cohesin binding causes the release of paused Pol2 on
247 LC-DICs.
248 Interestingly, siRad21 did not largely affect Pol2ser2 binding. Pol2ser2 levels on LC-DICs showed
249 no obvious difference between WT and siRad21 cells (Figs. 3d-f). In KD_Ctrl cells, there was no more
250 stalling at LC-DICs, but there was also no stimulating effect of E2; thus Pol2ser2 did not change from
251 WT_Ctrl to KD_Ctrl. In KD_E2 cells, transcription was activated by E2 stimulation but was limited by the
252 loss of cohesin on TSSs, and thus Pol2ser2 binding changed slightly from WT_E2 to KD_E2. To explore
253 changes in the expression level of genes that harbor LC-DICs after siRad21 treatment, we conducted
254 RNA-seq with siRad21 (Supplementary Fig. 6f). Without E2 treatment, siRad21 did not significantly affect
255 gene expression (p=0.23, KD_Ctrl as compared with WT_Ctrl). After E2 treatment, siRad21 moderately
256 affected gene expression (p=0.005, KD_E2 as compared with WT_E2), possibly because only a subset
257 of Pol2 that had paused on LC-DICs represented productive Pol2. We also quantitatively compared Pol2
258 and Pol2ser2 signals under four different conditions on various cohesin sites (Fig. 3f, Supplementary Fig.
259 6g). The results confirmed the significantly reduced bindings of Pol2 in WT_E2, KD_Ctrl and KD_E2 as
260 compared with WT_Ctrl cells (Fig. 3f, Mann–Whitney *U*-test, one-sided). Such a tendency was distinct
261 from those involving the TSSs of E2-responsive genes, up-regulated and non-changed intragenic
262 cohesin, other cohesin sites, and also other enhancer sites. Our results suggested that the role of
263 LC-DICs involves Pol2 pausing, which is different from the known roles of other cohesin sites.

264 In Figs. 1g-h, we showed the elevated binding of many TFs on DICs. To investigate whether the
265 increased binding of multiple TFs is caused by a decrease in cohesin binding, we generated ChIP-seq
266 data for CBP, P300 and Mau2 from siRad21 cells. Remarkably, a cohesin deficiency resulted in stronger
267 binding of those TFs at LC-DICs, which surpassed the level in ER-stimulated WT cells (dashed arrow in
268 Fig. 3g, Supplementary Fig. 7a-b). In contrast, there was little effect at the other intragenic enhancer site
269 (Fig. 3g). Considering that E2 stimulation recruits TFs by estrogen responsive elements in WT cells, the
270 increased binding of TFs in non-E2-stimulated siRad21 cells suggested that cohesin suppresses TF
271 binding at LC-DICs in some way, and this suppression is removed by the loss of cohesin, which is
272 followed by increased TF localization. Considering the chromatin de-compaction by E2 stimulation
273 shown in Fig. 1e, the increased binding of TFs at LC-DICs can be, at least in part, explained by a more
274 accessible chromatin structure near the LC-DICs, which is induced by the disruption of cohesin-mediated
275 interactions.
276
277 *Machine learning analysis of DIC features*
278 To confirm our findings, we implemented machine learning (ML) approaches (Supplementary Fig.
279 8a). We generated an integrated data matrix consisting of 175 features from genomic, transcriptomic and
280 epigenomic data for all cohesin sites (Supplementary Table 5; Methods). Especially, this matrix includes
281 features related to genomic location (e.g., intragenic or TSS) and to perturbation by E2 stimulation such
282 as Mvalue and ΔDLR. Supplementary Fig. 8b showed a Pearson correlation heatmap followed by
283 hierarchical clustering between all-by-all features for DICs or all cohesin sites. The 175 features resulted
284 in clear clusters both among DICs and among all cohesin sites (dashed boxes of different colors). We
285 annotated the clusters as promoter, enhancer, enhancer-promoter interaction (E-P), insulator and
286 chromatin architecture. As compared with all cohesin sites, DICs showed lower co-binding tendency in
287 the promoter cluster and higher co-binding in the enhancer and E-P clusters. This showed the
288 effectiveness of our matrix in distinguishing DICs from other cohesin sites.
289 We then applied unsupervised k-means clustering (k = 10) to the matrix and obtained 10 clusters for
290 all cohesin sites (cluster 0–9, Fig. 4a, Supplementary Fig. 10), among which only cluster 4 and cluster 7
291 showed intragenic cohesin binding that decreased after E2 stimulation, indicating the DIC-like clusters
292 (Fig. 4b). We identified the following characteristics of cluster 4 (Fig. 4c, upper): 1) co-binding with
293 tissue-specific TFs (e.g., ER and FOXA1), 2) enrichment of enhancer markers and Pol2, 3) relatively low
294 intensity of cohesin and CTCF peaks and 4) chromatin de-compaction. Therefore, cluster 4 represented
295 the LC-DIC-like cluster. In contrast, cluster 7 (Fig. 4c, lower) showed the following characteristics: 1) lack
296 of TF co-binding, 2) high intensity of CTCF peaks and 3) highly related to topological boundaries and

297 chromatin architecture features (e.g., TAD borders, Hi-C loops). Therefore, cluster 7 represented the
298 HC-DIC-like cluster. Compared with "CNC-like" intragenic cohesin sites[5, 6] (clusters 2, 3 and 8;
299 Supplementary Fig. 10), cluster 4 (LC-DICs) co-localized only with enhancer markers and several master
300 regulators (FOXA1, ER and GATA3), and therefore it is distinct from typical *cis*-regulatory modules
301 (CRMs) at which many TFs co-localize. In contrast, cluster 7 (HC-DICs) consists of a cluster of intragenic
302 cohesin sites that tend to be localized to open chromatin, are highly de-compacted and contain loops but
303 are strongly negatively correlated with TFs. Therefore, they may be associated with a more universal
304 chromatin structure that is required for proper gene transcription.

305 To further explore the characteristics of DICs, we applied modeling of supervised ML (logistic
306 regression, support vector machine, and random forest) to predict LC- and HC-DICs from all cohesin
307 sites in a binary manner (labeled by 0 or 1). In this analysis, the input matrix consisted of 168 features
308 (features related to genomic location, cohesin changes and CTCF signal were excluded). We selected
309 chromosomes 16 to 22 for testing, and the remaining chromosomes were divided into training and
310 validation by five-fold cross-validation (see Methods). Because DICs are a small subset of all cohesin
311 sites, we used SMOTE over-sampling[28] to deal with such "imbalanced" classifications. The trained model
312 that was based on logistic regression achieved the best performance overall as compared with the others
313 (Supplementary Figs. 8c-d) and also performed adequately with the test data (Supplementary Fig. 8e).
314 Finally, we identified important features for the prediction of LC-DICs and HC-DICs by calculating the
315 relative feature importance from the trained model (Figs. 4d-e). LC-DICs were positively associated with
316 1) enhancer markers (H3K27ac, H3K4me1, P300); 2) Pol2 peaks, the Pol2-pausing regulator (LARP7)[29]
317 and a transcriptional repressor (ZBTB1)[30]; 3) tissue-specific regulators (FOXA1[26], HSF1[31], ER[18]). Both
318 LC-DICs and HC-DICs were positively associated with open chromatin (FAIRE-open, DNase-open) and
319 chromatin de-compaction (ΔDLR), and were negatively associated with H3K27me3 and CpG island
320 levels. HC-DICs, in particular, showed positive features of Hi-C loops but negative features of Pol2 loops
321 and TF binding, which is consistent with our analysis above, indicative of the TF-independent chromatin
322 de-compaction. Taken together, the application of machine learning successfully isolated special subsets
323 of cohesin sites (DICs) from all cohesin sites, which also provided us with additional characteristics by
324 which they can be identified.
325
326 *Characterization of DIC tissue specificity*

327 As DICs were enriched by many tissue-specific factors, we wondered whether our observations
328 about DICs were consistent with other tissues or cell types. We generated Rad21 ChIP-seq for 293T
329 cells (kidney), B-cells (lymphocytes), human skin fibroblast cells, RPE (retinal pigmented epithelium)

330 cells, and HeLa cells (cervical cancer). Cohesin peaks at MCF-7 derived LC-DICs were more specific in
331 MCF-7 cells, whereas cohesin peaks at HC-DICs were more ubiquitous across cell types (Figs. 5a-b).
332 We then asked whether HC-DICs play a role in tissue-specific transcription. Across cell types, the peak
333 intensities for Rad21 at HC-DICs were negatively correlated with transcription levels of their host genes
334 (Fig. 5c, Supplementary Fig. 9a), suggesting that genes with stronger HC-DIC binding had lower
335 transcription activities. Therefore, HC-DICs also showed the ability to impede transcription, which is
336 consistent with our motif analysis above.

337 To confirm whether DICs in other cell types also exhibit similar characteristics, we performed
338 ChIP-seq experiments on RPE cells with FBS (fetal bovine serum) and DRB (5,6-dichloro-1-β-D-
339 ribofuranosylbenzimidazole), which function as a stimulator and inhibitor of transcription[32], respectively.
340 First, we tested if the ML model trained by MCF-7 data was applicable to the RPE data. We used 25
341 features that were available for both MCF-7 and RPE cells to predict whether binding of an intragenic
342 cohesin was decreased or not after transcription stimulation (Fig. 5d). The predicted DICs overlapped
343 extensively with the experimentally determined ones ($p < 10^{-161}$, hypergeometric test), indicating that
344 DICs exhibited some common rules across cell types. Then we identified DICs of stimulation-responsive
345 genes in RPE cells (Supplementary Fig. 9b). Similar to DICs in MCF-7 cells, RPE derived DICs also
346 showed tissue-specific binding patterns (Supplementary Fig. 9c). FBS stimulation decreased the
347 intensity of cohesin (Rad21 and SA1) at DICs (position H1 to H2, L1 to L2 in Fig. 5e; Supplementary Fig.
348 9d), whereas transcriptional inhibition by DRB increased it. In addition, further treatment with DRB (i.e.,
349 FBS+DRB) reverted the decrease in cohesin binding caused by FBS stimulation (H2 to H5, L2 to L5 in
350 Fig. 5e; Supplementary Fig. 9d). Moreover, RNA Pol2 stalling and the release of paused Pol2 were also
351 observed at LC-DICs in RPE cells (Fig. 5e, Supplementary Fig. 9e). In addition, LC-DICs, but not
352 HC-DICs, co-bound with enhancer marks and several TFs. Thus, DICs are not a phenomenon
353 associated with only breast cancer cells but also are found in normal human cell lines.

354

355 *Analysis of DICs in CdLS and CHOPS cells*

356 Finally, we attempted to examine the participation of DICs in the observed phenotypes in individuals
357 with CdLS and CHOPS. To this end, we generated ChIP-seq data from patient-derived fibroblast cells,
358 together with the data that were generated in our previous study[17]. We overlapped the binding sites of
359 intragenic cohesin in different cell types (Fig. 5f). Whereas most sites were shared among samples, there
360 were 332 Rad21 sites that were absent in both CdLS and CHOPS cells, which we defined as DICs.
361 RNA-seq analysis showed that host genes of DICs (both LC- and HC-DICs) in both CdLS and CHOPS
362 cells showed a significant increase in transcription (Fig. 5g, Supplementary Fig. 9f; paired t-test),

363 suggesting that the decreased cohesin binding at DICs was correlated with expression upregulation in
364 both CdLS and CHOPS. We also assessed the binding of TFs at 185 LC-DICs and 147 HC-DICs (Fig. 5h,
365 Supplementary Fig. 9g). Interestingly, at LC-DICs, the peak intensity of AFF4 (causative gene of CHOPS)
366 increased in both CdLS and CHOPS cells, whereas lower binding of NIPBL (causative gene of CdLS)
367 was observed only in CdLS cells (Fig. 5h). Enhancer marker H3K27ac was highly enriched but did not
368 change among the three cell types, whereas Pol2 and Pol2ser5 (RNA pol II CTD phospho Ser5, which
369 represents paused Pol2) decreased in both CdLS and CHOPS cells, which is consistent with our
370 observations in MCF-7 and RPE cells. Taken together, this result suggests that DICs, especially
371 LC-DICs, are involved in abnormal transcription associated with both CdLS and CHOPS. As both CdLS
372 and CHOPs are involved in abnormal Pol2 regulation[33], LC-DICs might offer a common pathogenetic
373 mechanism. Based on the observations, we concluded that intragenic cohesin sites can be a good
374 candidate to investigate and link the phenotypes of these two cohesinopathy disorders.
375

376 **Discussion**

377 Cohesin is thought to be responsible for transcription regulation and chromatin folding. Several
378 models have been proposed to explain its functions. Cohesin can mediate enhancer-promoter loops with
379 the mediator complex or can function as a blocker between enhancer and promoter in conjunction with
380 insulator factor CTCF[34]. Cohesin also participates in the formation of chromatin topological structures via
381 the loop extrusion model[8]. A recent paper reported that transcription stimuli such as IFN-beta in THP-1
382 cells can displace cohesin from chromatin[10], which attracted our interest. Here, we focused on intragenic
383 cohesin, a subset of cohesin that was scarce, if not none, discussed in previous research. Of note, we
384 emphasized the effect of negative regulation of gene expression by cohesin-mediated chromatin loops,
385 whereas most of the previous studies implicitly assumed the positive regulation of expression by these
386 loops. DICs were negatively associated with activated transcription and chromatin compaction. Whereas
387 LC-DICs were highly enriched with enhancer markers and paused Pol2, HC-DICs were more involved in
388 the features of chromatin architectures. Importantly, DICs could be found in multiple cell types, especially
389 in CdLS and CHOPS cells, which partly supported the similarities between CdLS and CHOPS.

390 Chromatin interactions are required not only to facilitate transcription but also for Pol2 pausing[35]. By
391 using siRad21 cells, we confirmed that the release of Pol2 was related to the loss of cohesin at LC-DICs,
392 which supported our model that intragenic loops formed by cohesin paused Pol2 and that transcription
393 elongation from TSSs could remove such cohesin and then release the paused Pol2 (Fig 5i). Notably, we
394 did not observe significant changes in the expression of genes that host LC-DICs by siRad21
395 (Supplementary Fig. 6f). As most LC-DICs are located in intronic regions, Pol2 released from LC-DICs

396 might be involved in accurate RNA splicing. Notably, a recent study suggested that intragenic enhancers,
397 in addition to activating genes, also attenuate the transcription of their host genes during productive
398 elongation[12], which evokes the functional link between LC-DICs and Pol2 pausing. In contrast, HC-DICs
399 showed a high preference for loop occurrence mediated by CTCF, possibly to play a role in topological
400 boundaries (e.g., sub-TADs). Across different cell types and genes, the Rad21 signal at HC-DICs was
401 negatively correlated with the expression of host genes, indicating the role of HC-DICs in restraining
402 transcription. Whereas we observed that more than half of HC-DIC–mediated loops anchored intronic
403 regions of two genes, it was difficult to infer the biological meaning of this because HC-DICs scarcely
404 overlapped with any other TFs. Further biological approaches such as genome editing of HC-DICs of
405 activated genes could be promising in the future.

406 Modifications at intragenic regions affect transcription events. For instance, intragenic methylation
407 can prevent spurious transcription initiation[11]; Intragenic microRNAs affect the expression of their host
408 genes[13]. Here we present the first study that focused on intragenic cohesin sites. We also used penalty
409 linear regression followed by univariate linear regression to better understanding the changes of cohesin
410 bindings in intragenic regions (see Method and Supplementary Fig. 8f-h). Apart from the decreased ones,
411 the increased intragenic cohesin sites seemed to be also correlated with many important features, as
412 they are positively predicted by ER and several TFs. Although we characterized intragenic cohesin sites
413 that showed decreased bindings in this study, all types of intragenic cohesin might have a role in
414 transcription regulation. In addition, Kowalczyk et al. point out that intragenic enhancers can act as
415 alternative promoters[36]. Our DICs did not overlap with any known alternative promoters. Even though we
416 know little about the molecular mechanism, our results strongly suggest a previously undescribed
417 function of cohesin in intragenic regions with respect to gene expression regulation.

418 In summary, large-scale multi-omics enabled us to identify a cluster of cohesin DICs in MCF-7 and
419 other cell types. Some tissue-specific DICs (LC-DICs) were related to enhancers and Pol2
420 pausing/release, whereas others (HC-DICs) contributed to chromatin architecture and might attenuate
421 transcription. Our integrated analysis and machine learning approaches indicated distinct characteristics
422 that distinguish DICs from other cohesin binding sites. Based on these genomic, epigenomic and
423 transcriptomic characteristics, we can infer that DICs have distinct functions as compared with other
424 cohesin sites.

425

426 **Methods**

427 *Cell culture and treatment*

428 RPE cells[37] and MCF-7 cells (JCRB Cell Bank) were cultured in DMEM containing 10% FBS and 1%
429 penicillin/streptomycin. Before subsequent treatments, RPE cells were cultured in serum-free medium for
430 48 hours and then were incubated in DMEM containing 10% FBS for 30 min. MCF-7 cells were
431 maintained in phenol red–free medium containing charcoal-dextran–stripped FBS (Life Technologies) at
432 70–80% confluency for 2 days before treatment with 50 nM E2 (SIGMA) for the indicated times. Rad21
433 siRNA oligos[4] were transfected using Lipofectamine RNAiMax (Life Technologies) according to the
434 manufacturer's instructions at 40 hours before treatment with E2. DRB (TCI) was added at 1.5 hours
435 before treatment with E2. The effect of cohesin (Rad21)-deficiency were verified by western blot as
436 shown in Supplementary Fig. 6e.
437
438 *ChIP and antibodies*
439 Cells were fixed in medium or phosphate buffered saline with 1% formaldehyde at room
440 temperature for 10 min. ChIP experiments were performed as described[38]. ChIP-seq libraries were
441 prepared using NEBNext ChIP-seq Library Prep Master Mix Set for Illumina (New England BioLabs).
442 Rabbit polyclonal antibody for Rad21 has been described in[39]. Antibody for Pol2 (#14958) was from Cell
443 Signaling Technology. Antibodies for Mau2 (ab46906) and SA1 (ab4457) were from Abcam. Antibodies
444 for TAF (A303-505A) and AFF4 (A302-538A) were from Bethyl Laboratory. CTCF (07-729) antibody was
445 from Merck Millipore. Antibodies for Pol2ser2 and H3K27ac were kindly provided by Dr. H Kimura
446 (TITech). Antibodies for P300 (sc-585) and Med1 (sc-5334) were from Santa Cruz Biotechnology.
447 Antibody for CBP (606402) was from BioLegend.
448
449 *ChIP-seq analysis*
450 After quality check by FastQC and SSP[40], ChIP-seq reads were aligned to the human reference
451 genome (hg38) using Bowtie[41] version 1.2.2 with "-n2 -m1" parameters, by which we considered only
452 uniquely mapped reads and allowed two mismatches in the first 28 bases per read. Peak calling was
453 performed using MACS2[42] version 2.2.6 with default settings. We used DROMPA[43] version 3.7.2 to
454 conduct statistical analysis and visualization. For visualization of ChIP-seq binding to particular
455 chromatin regions, reads were normalized relative to total read number, and gene annotation was
456 obtained from NCBI reference sequences (RefSeq; hg38). Read profiles around the sites of interest were
457 plotted with the PROFILE mode of DROMPA, whereas the heatmap of target sites (2.5 kb around the
458 peak summit) was plotted using HEATMAP mode. Genomic distribution in Fig. 2e was plotted by
459 ChIPseeker[44]. Downstream analysis, such as peak overlap, was performed by Bedtools[45] version 2.29.2

460 and Samtools[46] version 1.9. Sources for all ChIP-seq data and other next-generation sequencing data
461 (including our data and public data) are listed in Supplementary Tables S2-3.
462
463 *Hi-C analysis*
464 All in-situ Hi-C data (control or E2-treated MCF-7 cells with two replicates) were aligned to the hg38
465 human reference genome. Further analysis was carried out mainly by Juicer[22] version 1.11.04. All
466 contact matrices were normalized by the KR method in Juicer. Chromatin loops were annotated using the
467 HiCCUPS algorithm with default parameters[22]. The loop regions we used were merged from the results
468 of 5-kb,10-kb and 25-kb resolutions. Aggregate peak analysis (APA) was performed using the 'apa'
469 mode of Juicer (5-kb resolution), to measure the enrichment of the Hi-C signal around a set of peaks.
470 The visualization of the contact matrix on the *MREG* locus was accomplished by Matplolib. After
471 correction and normalization, comparable contact matrices were plotted at a 5-kb resolution. We merged
472 two adjacent bins for smoothing. Other Hi-C analyses were performed using HOMER[10]. We made the
473 Tag directory with the "GATC" restriction site sequence. Chromatin compaction scores ΔDLR and ΔICF
474 were calculated for each 5-kb region across the genome (-res 5000) from a 15-kb window size (-window
475 15000). Other metrics including PC1, insulation score and TAD boundaries were obtained using HOMER
476 with default parameters. We used the WashU epigenome browser[47] to visualize Supplementary Fig. 3b.
477
478 *ChIA-PET analysis*
479 RNA polymerase II–bound chromatin interactions in MCF-7 cells were extracted from ChIA-PET
480 data (GSE33664). All fastq files were applied to the published pipeline Mango[48] with default parameters,
481 based on the hg38 reference genome. ChIA-PET interactions were visualized by DROMPA with the
482 parameter '-inter'.
483
484 *RNA-seq and GRO-seq analysis*
485 Using HISAT2[49] version 2.2.0, we aligned paired-end RNA-seq reads to the index established from
486 the hg38 reference genome. The output SAM files were converted to BAM files by Samtools. Htseq[50]
487 version 0.11.3 was then used with default parameters to generate a count table, which describes the
488 number of reads on each gene. We used a GTF file (GRCh38.p12) from GENCODE for gene annotation.
489 Subsequent differential expression analysis was achieved using DESeq2[51], with its internal normalization.
490 For GRO-seq, alignment was carried out using Bowtie with "-n2 -m1" parameters. The output was
491 preprocessed and visualized using DROMPA.
492

493 *Data collection and machine learning*

494 All datasets used in machine learning are listed in Table S5. Apart from our data, public omics data
495 in wild-type MCF-7 cells were downloaded mainly from the GEO database, ENA database, ENCODE
496 project, FANTOM5 project, UCSC genome browser and GWAS Catalog database. These data were then
497 overlapped with all 184,140 cohesin peaks. As a result, we obtained 15 continuous features and 160
498 binary features, the latter of which indicated whether a kind of data was co-localized (1) or not
499 co-localized (0) at a cohesin site. After normalization of continuous features, the big matrix, which
500 consisted of 184,140 rows (cohesin sites) and 175 features, was imported into for different analyses. The
501 features correlation heatmap for all cohesin sites and DICs was made with the R package *corrplot*. We
502 used scikit-learn version 0.22.1 to perform machine learning. Overall, the parameters used in scikit-learn
503 were optimized by grid search with 5-fold cross-validation. For unsupervised learning (k-means), all 175
504 features were used to fit models. For supervised learning (logistic regression, support vector machine,
505 random forest), we omitted Mvalue, cohesin location and CTCF signal information and then used the
506 remaining 168 features as independent variables $X_i = (X_{i1}, X_{i2}, \dots, X_{ij})$, for $i = 1, 2, \dots, 184140$ and $j =$
507 $1, 2, \dots, 168$. Based on whether they were DICs or not, we labeled each cohesin site as 1 or 0 and then
508 used it as a dependent variable $Y_i \in \{0, 1\}$. The conditional probability of logistic regression was
509 calculated as follows:

510 $$P(Y_i = 1|X = X_i) = \frac{1}{1 + e^{-(\beta_0 + \sum_{j=1}^{168} \beta_j X_{ij})}}$$

511 where β_j is the regression coefficient of each feature. We used training data to do model fitting and
512 used test data to validate model performance. To apply the MCF-7–derived ML model to RPE cells, we
513 used 25 features that were available in both MCF-7 and RPE cells. We used logistic regression with L1
514 penalty to decide whether each intragenic cohesin site had decreased binding (1) or not (0). Then the
515 MCF-7–fitted model was applied to the RPE features to predict DICs.

516 We also applied penalized regression followed by univariate linear regression as described[52], to
517 reveal which features contributed to negative or positive Mvalue (log ratio of cohesin peak intensity
518 between E2 and control) in intragenic cohesin (26066 sites). We used 169 features (of the 175 features,
519 6 were excluded: 5 features related to cohesin position and the Mvalue feature) as independent variables
520 $X_i = (X_{i1}, X_{i2}, \dots, X_{ij})$, for $i = 1, 2, \dots, 26066$ and $j = 1, 2, \dots, 169$, whereas the Mvalue was the dependent
521 variable Y_i. Instead of using the ordinary least squares approach, we used the elastic net loss function:

522 $$L_{enet}(\hat{\beta}) = \frac{\sum_{i=1}^{n}(y_i - x_i'\hat{\beta})^2}{2n} + \lambda\left(\frac{1-\alpha}{2}\sum_{j=1}^{169}\hat{\beta}_j^{\,2} + \alpha\sum_{j=1}^{169}|\hat{\beta}_j|\right)$$

523 to the linear model $Y_i = \beta_0 + \sum_{j=1}^{169} \beta_j X_{ij}$, where $n = 26066$ and $\hat{\beta}$ was the estimation of β. λ was
524 chosen by cross-validation, and $\alpha = 0.5$ was used to consider both the L1 and L2 penalty. Feature
525 selection with such regularization was useful for filtering out non-significant or redundant features. The
526 remaining features were applied to univariate linear regression $Y = a + bX$ to calculate the regression
527 coefficient (Supplementary Figs. 8f–h).
528
529 *Extraction of DICs*
530 Quantitative comparison of Rad21 binding events was performed using MAnorm[19] version 1.3.0
531 with default parameters. This results in the normalized Mvalue, a quantitative measure of differential
532 binding for all cohesin sites. To acquire more convincing sites, we combined our results with high-quality
533 ChIP-seq data from E-TABM-828[5]. Criteria for selecting decreased peaks were peak width < 3 kb and
534 Mvalue < −0.5. Next, we used RefSeq as the reference genome to obtain intragenic regions. As
535 described in Supplementary Fig. 1e, we excluded 10kb flanking regions around TSS and TES. Only large
536 genes (gene length > 20 kb) were considered. E2-responsive genes were defined as genes with an
537 increased Pol2ser2 ChIP-seq signal (ratio > 1.2) in the presence of E2 relative to control and that were
538 validated by RNA-seq data. Decreased peaks at intragenic region of 499 E2-responsive gene were
539 defined as DICs. Next, to quantify CTCF read density on DICs, we used MULTICI options in DROMPA
540 software. Peaks with extremely low Rad21 signals were omitted. Finally, we separated the DICs into 141
541 high-CTCF DICs (HC-DICs) and 417 low-CTCF DICs (LC-DICs).
542
543 *Motif analysis*
544 Motifs were analyzed using HOMER. Briefly, peak files in standard bed format were converted to
545 HOMER peak files, and then the command *findMotifsGenome.pl* was used to discover the motif. The
546 results included known motifs as well as *de novo* discovered motifs. The size of the region used for motif
547 finding was set to 200 bp. The top 10 motifs with the lowest *q*-values (Benjamini-Hochberg) are shown.
548
549 *Software environment*
550 All analyses were based on Ubuntu 18.04.4 with Python 3.6.9 and R 3.6.3. Data were processed
551 using R base package or Numpy (v 1.17.2) as well as Pandas (v 0.25.1) in Python. Figures were drawn
552 with DROMPA (v 3.7.2), Matplotlib (v 3.1.1), ggplot2 and R base plotting.
553
554 **Abbreviations:**

ChIP-seq: chromatin immunoprecipitation followed by sequencing; CNCs: cohesin-non-CTCF sites; RNA-seq: RNA sequencing; Hi-C: high-throughput chromosome conformation capture; ChIA-PET: chromatin interaction analysis by paired-end tag sequencing; DIC: decreased intragenic cohesin; LC-DIC: low-CTCF decreased intragenic cohesin; HC-DIC: high-CTCF decreased intragenic cohesin. Pol2: RNA polymerase II; Pol2ser2: RNA pol II CTD serine-2 phosphorylation; TSS: transcription start site; TES: transcription end site; TAD: topologically associating domain.

Competing interests:

The authors declare that they have no competing interest.

Author contributions

J.W. performed all bioinformatics analysis. R.N. conceived this project. J.W. and R.N. drafted the manuscript. M.B. prepared ChIP-seq and RNA-seq samples. K.S. supervised the sample preparation and sequencing, suggested ways to improve the analysis, and improved the manuscript.

Data availability

The raw sequencing data and processed files are available at the GEO

References:

1. Kim Y, Shi Z, Zhang H, Finkelstein IJ, Yu H. Human cohesin compacts DNA by loop extrusion. *Science* **366**, 1345-1349 (2019).
2. Nishiyama T. Cohesion and cohesin-dependent chromatin organization. *Current opinion in cell biology* **58**, 8-14 (2019).
3. Bloom MS, Koshland D, Guacci V. Cohesin Function in Cohesion, Condensation, and DNA Repair Is Regulated by Wpl1p via a Common Mechanism in Saccharomyces cerevisiae. *Genetics* **208**, 111-124 (2018).
4. Wendt KS*, et al.* Cohesin mediates transcriptional insulation by CCCTC-binding factor. *Nature* **451**, 796-801 (2008).
5. Schmidt D*, et al.* A CTCF-independent role for cohesin in tissue-specific transcription. *Genome research* **20**, 578-588 (2010).
6. Faure AJ*, et al.* Cohesin regulates tissue-specific expression by stabilizing highly occupied cis-regulatory

587 modules. *Genome research* **22**, 2163-2175 (2012).
588 7. Kagey MH*, et al.* Mediator and cohesin connect gene expression and chromatin architecture. *Nature* **467**,
589 430-435 (2010).
590 8. Fudenberg G, Imakaev M, Lu C, Goloborodko A, Abdennur N, Mirny LA. Formation of Chromosomal
591 Domains by Loop Extrusion. *Cell reports* **15**, 2038-2049 (2016).
592 9. Dixon JR, Gorkin DU, Ren B. Chromatin Domains: The Unit of Chromosome Organization. *Molecular cell* **62**,
593 668-680 (2016).
594 10. Heinz S*, et al.* Transcription Elongation Can Affect Genome 3D Structure. *Cell* **174**, 1522-1536 e1522
595 (2018).
596 11. Neri F*, et al.* Intragenic DNA methylation prevents spurious transcription initiation. *Nature* **543**, 72-77 (2017).
597 12. Cinghu S*, et al.* Intragenic Enhancers Attenuate Host Gene Expression. *Molecular cell* **68**, 104-117 e106
598 (2017).
599 13. Hinske LC, Galante PA, Kuo WP, Ohno-Machado L. A potential role for intragenic miRNAs on their hosts'
600 interactome. *BMC genomics* **11**, 533 (2010).
601 14. Krantz ID*, et al.* Cornelia de Lange syndrome is caused by mutations in NIPBL, the human homolog of
602 Drosophila melanogaster Nipped-B. *Nature genetics* **36**, 631-635 (2004).
603 15. van der Lelij P*, et al.* Synthetic lethality between the cohesin subunits STAG1 and STAG2 in diverse cancer
604 contexts. *eLife* **6**, (2017).
605 16. Kon A*, et al.* Recurrent mutations in multiple components of the cohesin complex in myeloid neoplasms.
606 *Nature genetics* **45**, 1232-1237 (2013).
607 17. Izumi K*, et al.* Germline gain-of-function mutations in AFF4 cause a developmental syndrome functionally
608 linking the super elongation complex and cohesin. *Nature genetics* **47**, 338-344 (2015).
609 18. Theodorou V, Stark R, Menon S, Carroll JS. GATA3 acts upstream of FOXA1 in mediating ESR1 binding by
610 shaping enhancer accessibility. *Genome research* **23**, 12-22 (2013).
611 19. Shao Z, Zhang Y, Yuan GC, Orkin SH, Waxman DJ. MAnorm: a robust model for quantitative comparison of
612 ChIP-Seq data sets. *Genome biology* **13**, R16 (2012).
613 20. Bowman EA, Kelly WG. RNA polymerase II transcription elongation and Pol II CTD Ser2 phosphorylation: A
614 tail of two kinases. *Nucleus* **5**, 224-236 (2014).
615 21. Li X*, et al.* A unified mechanism for intron and exon definition and back-splicing. *Nature* **573**, 375-380
616 (2019).
617 22. Durand NC*, et al.* Juicer Provides a One-Click System for Analyzing Loop-Resolution Hi-C Experiments.
618 *Cell Syst* **3**, 95-98 (2016).
619 23. Ren G*, et al.* CTCF-Mediated Enhancer-Promoter Interaction Is a Critical Regulator of Cell-to-Cell Variation

620 of Gene Expression. *Molecular cell* **67**, 1049-1058 e1046 (2017).
621 24. Lalmansingh AS, Karmakar S, Jin Y, Nagaich AK. Multiple modes of chromatin remodeling by Forkhead box
622 proteins. *Biochimica et biophysica acta* **1819**, 707-715 (2012).
623 25. Fournier M*, et al.* FOXA and master transcription factors recruit Mediator and Cohesin to the core
624 transcriptional regulatory circuitry of cancer cells. *Scientific reports* **6**, 34962 (2016).
625 26. Hurtado A, Holmes KA, Ross-Innes CS, Schmidt D, Carroll JS. FOXA1 is a key determinant of estrogen
626 receptor function and endocrine response. *Nature genetics* **43**, 27-33 (2011).
627 27. Andersson R*, et al.* An atlas of active enhancers across human cell types and tissues. *Nature* **507**, 455-461
628 (2014).
629 28. Chawla NV, Bowyer KW, Hall LO, Kegelmeyer WP. SMOTE: synthetic minority over-sampling technique.
630 *Journal of artificial intelligence research* **16**, 321-357 (2002).
631 29. Frilander MJ, Barboric M. The Interlocking Lives of LARP7: Fine-Tuning Transcription, RNA Modification,
632 and Splicing through Multiple Non-coding RNAs. *Molecular cell* **78**, 5-8 (2020).
633 30. Matic I*, et al.* Site-specific identification of SUMO-2 targets in cells reveals an inverted SUMOylation motif
634 and a hydrophobic cluster SUMOylation motif. *Molecular cell* **39**, 641-652 (2010).
635 31. Santagata S*, et al.* High levels of nuclear heat-shock factor 1 (HSF1) are associated with poor prognosis in
636 breast cancer. *Proceedings of the National Academy of Sciences of the United States of America* **108**,
637 18378-18383 (2011).
638 32. Busslinger GA*, et al.* Cohesin is positioned in mammalian genomes by transcription, CTCF and Wapl.
639 *Nature* **544**, 503-507 (2017).
640 33. Piche J, Van Vliet PP, Puceat M, Andelfinger G. The expanding phenotypes of cohesinopathies: one ring to
641 rule them all! *Cell Cycle* **18**, 2828-2848 (2019).
642 34. Merkenschlager M, Nora EP. CTCF and Cohesin in Genome Folding and Transcriptional Gene Regulation.
643 *Annual review of genomics and human genetics* **17**, 17-43 (2016).
644 35. Ong CT, Corces VG. Enhancer function: new insights into the regulation of tissue-specific gene expression.
645 *Nature reviews Genetics* **12**, 283-293 (2011).
646 36. Kowalczyk MS*, et al.* Intragenic enhancers act as alternative promoters. *Molecular cell* **45**, 447-458 (2012).
647 37. Gallego-Paez LM*, et al.* Smc5/6-mediated regulation of replication progression contributes to chromosome
648 assembly during mitosis in human cells. *Molecular biology of the cell* **25**, 302-317 (2014).
649 38. Komata M, Katou Y, Tanaka H, Nakato R, Shirahige K, Bando M. Chromatin immunoprecipitation protocol
650 for mammalian cells. *Methods in molecular biology* **1164**, 33-38 (2014).
651 39. Minamino M*, et al.* Esco1 Acetylates Cohesin via a Mechanism Different from That of Esco2. *Current*
652 *biology : CB* **25**, 1694-1706 (2015).

653 40. Nakato R, Shirahige K. Sensitive and robust assessment of ChIP-seq read distribution using a strand-shift
654 profile. *Bioinformatics* **34**, 2356-2363 (2018).
655 41. Langmead B, Trapnell C, Pop M, Salzberg SL. Ultrafast and memory-efficient alignment of short DNA
656 sequences to the human genome. *Genome biology* **10**, R25 (2009).
657 42. Zhang Y*, et al.* Model-based analysis of ChIP-Seq (MACS). *Genome Biol* **9**, R137 (2008).
658 43. Nakato R, Itoh T, Shirahige K. DROMPA: easy-to-handle peak calling and visualization software for the
659 computational analysis and validation of ChIP-seq data. *Genes Cells* **18**, 589-601 (2013).
660 44. Yu G, Wang LG, He QY. ChIPseeker: an R/Bioconductor package for ChIP peak annotation, comparison
661 and visualization. *Bioinformatics* **31**, 2382-2383 (2015).
662 45. Quinlan AR, Hall IM. BEDTools: a flexible suite of utilities for comparing genomic features. *Bioinformatics* **26**,
663 841-842 (2010).
664 46. Li H*, et al.* The Sequence Alignment/Map format and SAMtools. *Bioinformatics* **25**, 2078-2079 (2009).
665 47. Zhou X*, et al.* Exploring long-range genome interactions using the WashU Epigenome Browser. *Nature*
666 *methods* **10**, 375-376 (2013).
667 48. Phanstiel DH, Boyle AP, Heidari N, Snyder MP. Mango: a bias-correcting ChIA-PET analysis pipeline.
668 *Bioinformatics* **31**, 3092-3098 (2015).
669 49. Kim D, Paggi JM, Park C, Bennett C, Salzberg SL. Graph-based genome alignment and genotyping with
670 HISAT2 and HISAT-genotype. *Nature biotechnology* **37**, 907-915 (2019).
671 50. Anders S, Pyl PT, Huber W. HTSeq--a Python framework to work with high-throughput sequencing data.
672 *Bioinformatics* **31**, 166-169 (2015).
673 51. Love MI, Huber W, Anders S. Moderated estimation of fold change and dispersion for RNA-seq data with
674 DESeq2. *Genome biology* **15**, 550 (2014).
675 52. Hu S*, et al.* ncHMR detector: a computational framework to systematically reveal non-classical functions of
676 histone modification regulators. *Genome biology* **21**, 48 (2020).
677

Figure 1

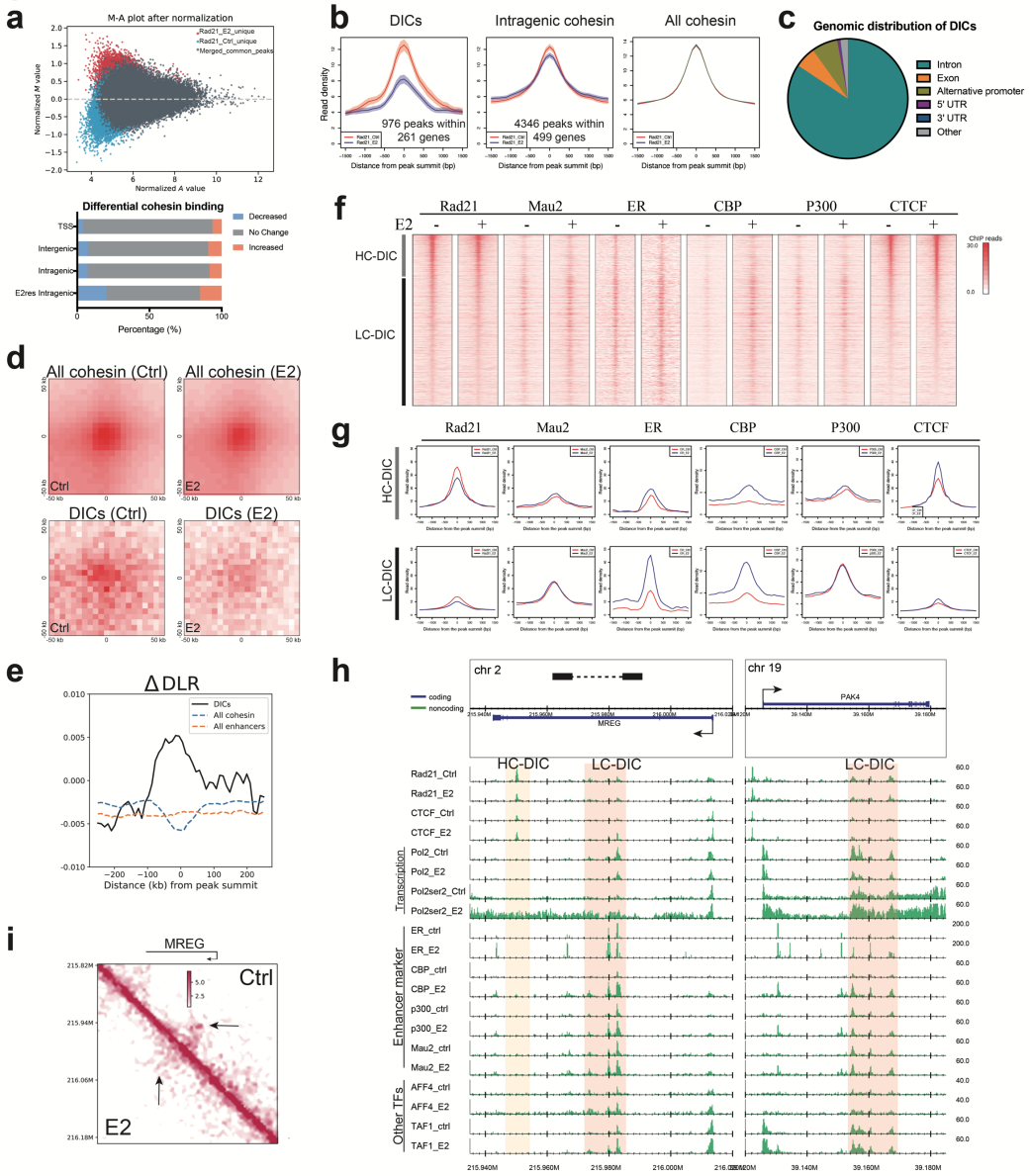

Fig. 1 Classification of decreased intragenic cohesin (DIC) sites. a. Quantitative comparison of cohesin peak intensity between control (Ctrl) and estrogen (E2)-treated MCF-7 cells. Mvalue is the $\log_2$(fold change) of normalized read densities under comparison. Avalue is the average signal strength of each peak. The lower panel shows the proportion of cohesin binding that decreased or increased. **b.** Average binding profiles on different cohesin sites. Red, control. Blue, E2 treatment. **c.** Genomic distribution of all DICs suggested most of DICs were located in introns. **d.** Aggregate peak analysis around DICs or all cohesin peaks at a 5-kb resolution. **e.** Chromatin compaction scores around DICs, all cohesin sites and all enhancers (summit ± 500 kb). ΔDLR (E2 vs. control) was calculated at a 25-kb resolution. **f.** Heatmap of ChIP-seq reads at DICs (peak summit ± 2.5 kb). CTCF (E2+) signal was used for sorting the order. DICs were divided into HC-DICs (gray bar) and LC-DICs (black bar). E2–, control;

E2+, estrogen treated. **g.** Average binding profiles (summit ± 1.5 kb) of Rad21 and TFs on HC-DICs (upper) and LC-DICs (lower). Reads were normalized relative to the whole genome. The same *y*-axis scale was used for each protein. **h.** Read distribution of Rad21 and TFs around *MREG* and *PAK4* loci. Areas shaded in pink and light yellow indicate LC-DICs and HC-DICs, respectively. All reads were normalized relative to the whole genome. **i.** Hi-C contact map (5-kb resolution) around *MREG*. Arrows show the disappearance of chromatin interactions after E2 stimulation. The loop anchor is shown as a black bar in 1h.

Figure 2

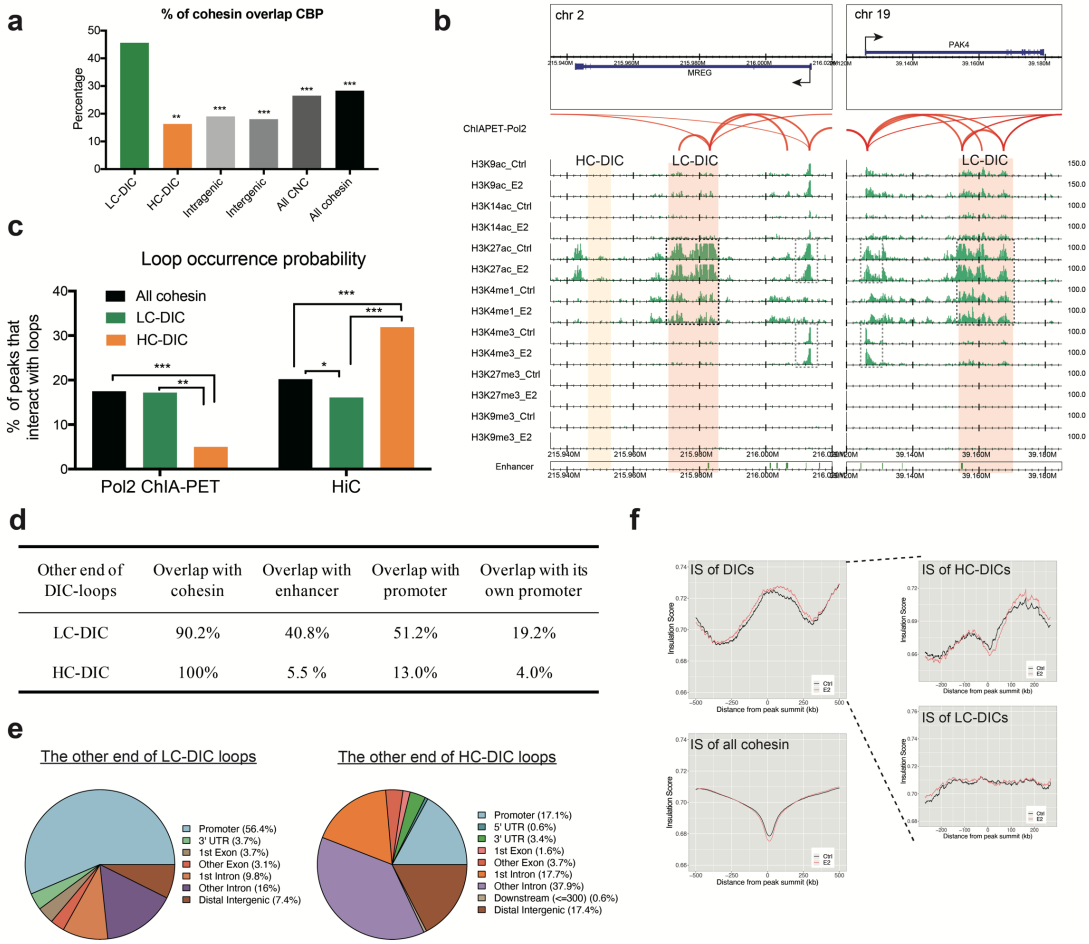

Other end of DIC-loops	Overlap with cohesin	Overlap with enhancer	Overlap with promoter	Overlap with its own promoter
LC-DIC	90.2%	40.8%	51.2%	19.2%
HC-DIC	100%	5.5 %	13.0%	4.0%

Fig. 2 Enhancers and loops on DICs. a. The proportion of cohesin overlap with CBP peaks. Fisher's exact test was used between LC-DICs and other cohesin sites. **$p < 10^{-5}$, ***$p < 10^{-10}$. **b.** Genomic binding of multiple histone markers. Enhancer markers H3K27ac and H3K4me1 (black dashed box) were enriched at LC-DICs. Gray dashed boxes indicate histone markers for promoters. Red arcs show Pol2-mediated loops. **c.** Loop occurrence probabilities on DICs, calculated based on Pol2 ChIA-PET or Hi-C data. We used Fisher's exact test to do statistical comparisons. *$p < 0.05$, **$p < 0.01$, ***$p < 0.001$. **d.** The percentage of HiC loops (LC-DICs and HC-DICs) that interacted with cohesin, enhancers, promoters or the promoter of their host gene. **e.** Genomic distribution of the other end of DIC-loops as generated by ChIPseeker. **f.** Insulation scores (ISs) for each 25-kb genomic region around DICs or all cohesin sites (summit ± 500 kb). DICs were further divided (dashed line) into HC-DICs and LC-DICs.

Figure 3

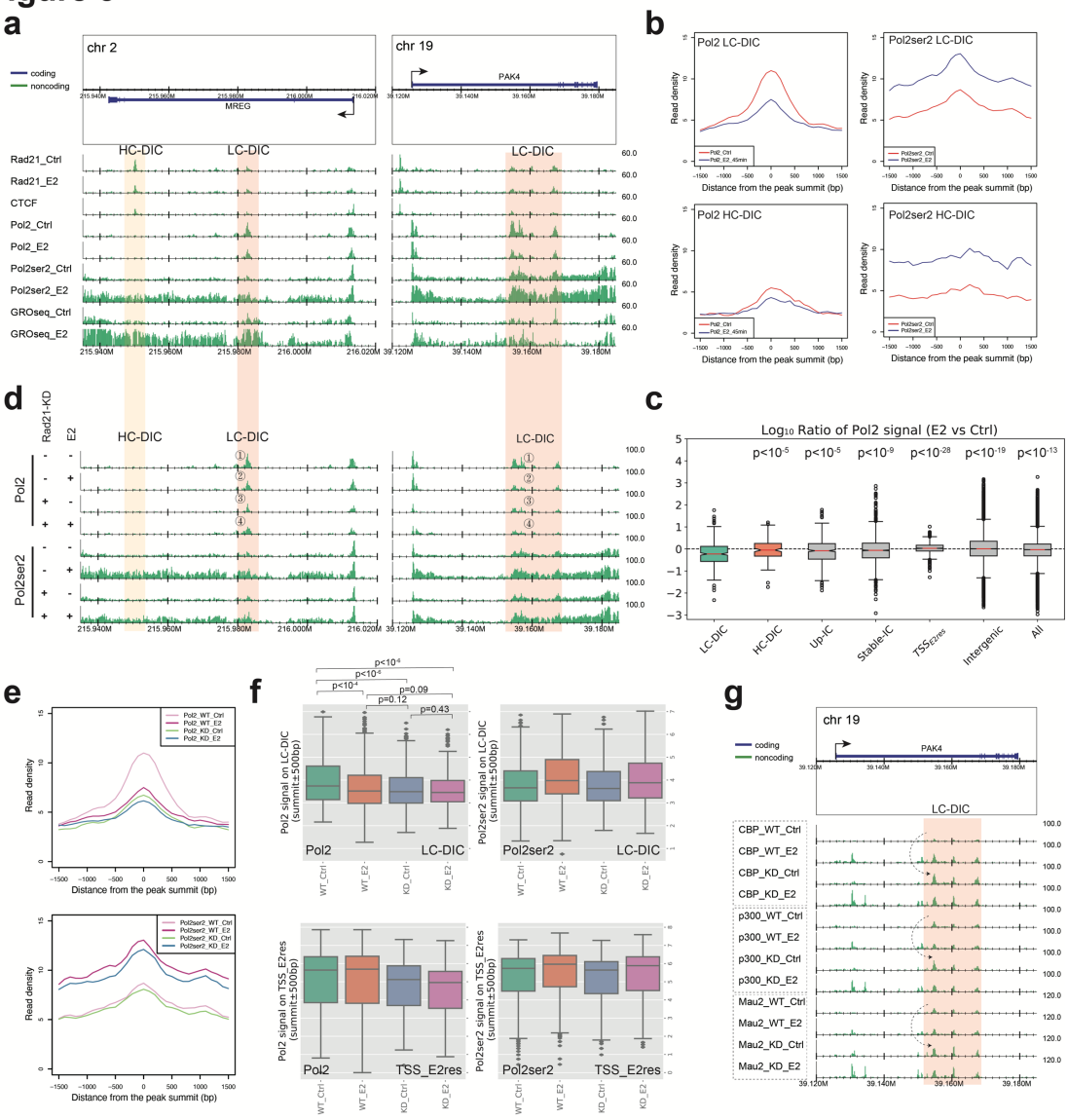

Fig. 3 Pol2 pauses on LC-DICs. a. Genomic binding of Pol2 and Pol2ser2 and GRO-seq data for *MREG* and *PAK4* loci. **b.** Binding profiles of Pol2 and Pol2ser2 on LC-DICs or HC-DICs, under control and E2 conditions. Reads were normalized relative to the whole genome**. c.** The $\log_{10}$ value of the ratio E2/Ctrl with respect to the Pol2 signal on various cohesin sites; *p*-values (Mann–Whitney *U*-test) were calculated between LC-DICs and other cohesin sites. Up-IC, up-regulated intragenic cohesin; stable-IC, unchanged intragenic cohesin; TSS_{E2res}, TSS of E2-responsive gene. **d.** Visualization of Pol2 and Pol2ser2 ChIP-seq data around *MREG* and *PAK4*. MCF-7 cells were treated as indicated. WT, wild type; KD, Rad21 knockdown; Ctrl, control; E2, estrogen. **e.** Pol2 and Pol2ser2 binding profiles around LC-DICs (summit ± 1.5 kb) under four different conditions. Reads were normalized relative to the whole genome. **f.** Quantitative comparison (Mann–Whitney *U*-test) of Pol2 and Pol2ser2 signals on LC-DICs or on TSSs of E2-responsive genes (TSS_E2res) under four different conditions. **g.** ChIP-seq results for CBP, P300

744 and Mau2 on *PAK4* gene in WT and Rad21 knockdown MCF-7 cells with the absence and presence of
745 E2 stimulation. Dashed arrows show increased binding events in cohesin-deficient cells.
746
747
748
749
750
751
752
753
754
755
756
757
758
759
760
761
762
763
764
765
766
767
768
769
770
771
772
773
774
775

Figure 4

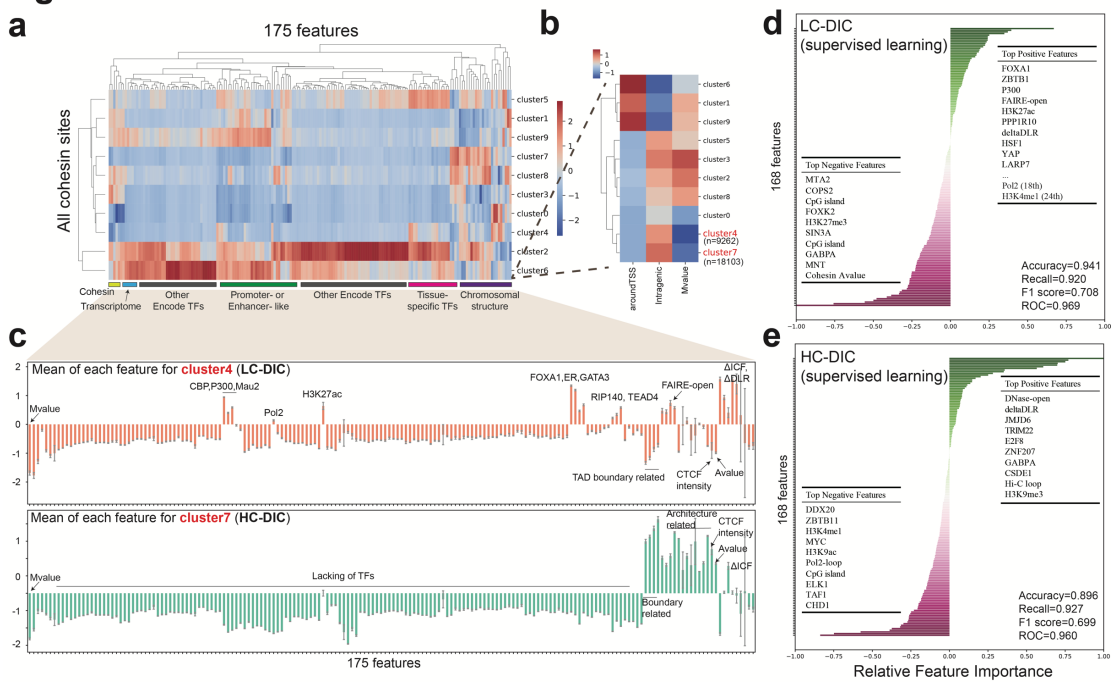

Fig. 4 Machine learning methods to classify DICs. a. Cluster heatmap by k-means (k = 10) methods. The 175 features were roughly classified into different groups. **b.** Magnified view of the heatmap area shown in A indicates three important features for these 10 clusters: "aroundTSS" indicates whether a cohesin site was near TSS; "intragenic" indicates whether a cohesin site was within a gene body; "Mvalue" is the $\log_2$ ratio of Rad21 peak density between the E2 and control group. **c.** The mean of each feature for cluster 4 and 7. The *y* axis shows the normalized (z-score) values of binary and continuous features. Error bars represent 95% confidence intervals. **d-e.** The importance of individual features from the logistic regression model for (**d**) LC-DICs and (**e**) HC-DICs. Top positive and negative features are listed inside the plots. Model performance is indicated in the bottom right.

Figure 5

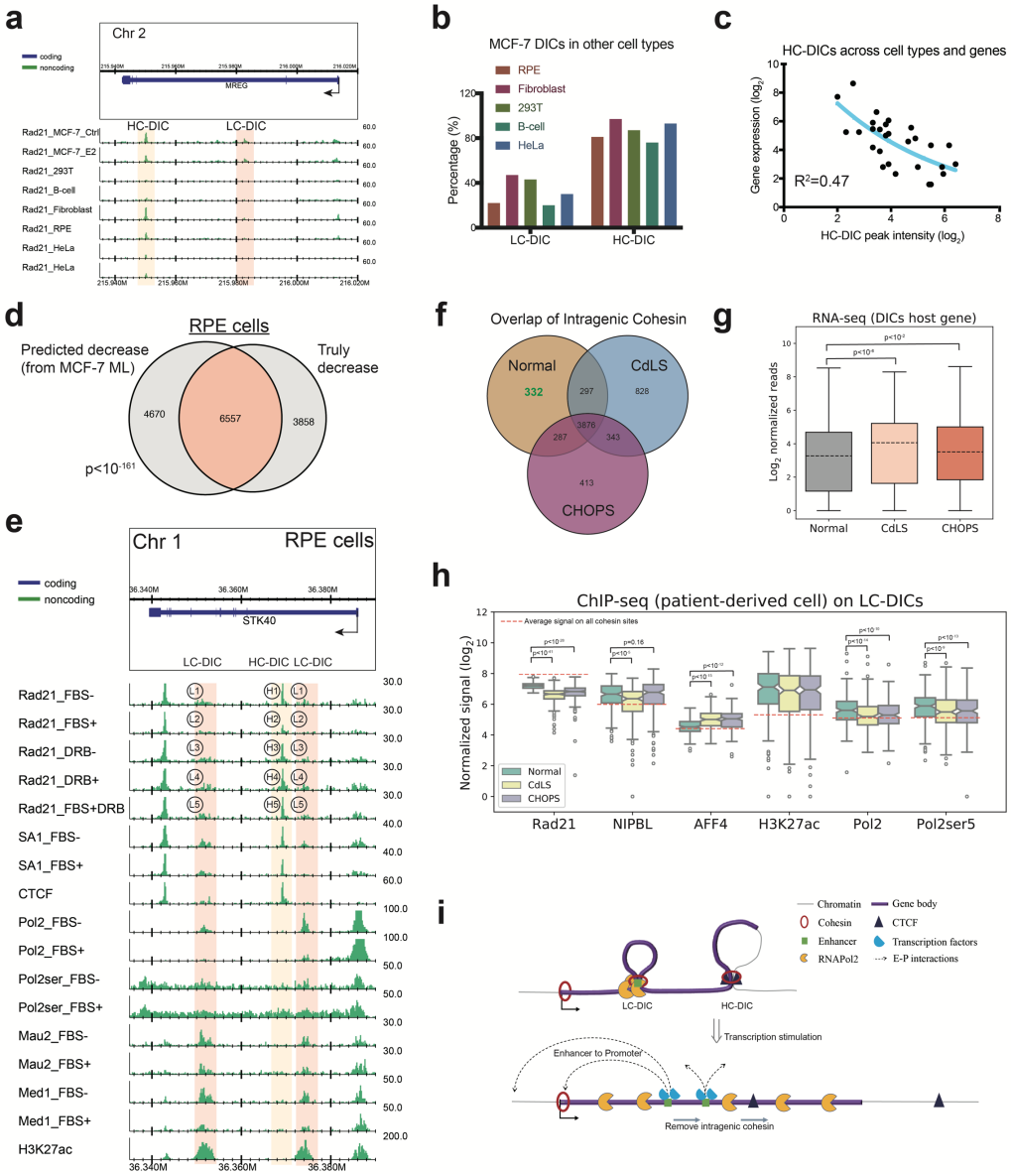

Fig. 5 DICs in other cell types. a. Rad21 ChIP-seq of the *MREG* locus in various cell lines (MCF-7, 293T, B-cells, Fibroblasts, RPE, HeLa). HC-DICs were observed in other cells but not LC-DICs. **b.** The percentage of MCF-7 DICs that could be found in other cell types. **c.** Relationships between peak density of HC-DICs and the expression of their host genes. Gene expression data for the different cell types were obtained from the GTEx database. **d.** Overlap between DICs that were predicted relative to those that were experimentally isolated; *p*-values were calculated with the hypergeometric test. **e.** ChIP-seq data of the example locus in RPE cells. L1-5 indicated LC-DIC sites and H1-5 indicated HCDIC sites. **f.** Overlap of intragenic cohesin sites in normal and CdLS- and CHOPs-derived fibroblast cells. **g.** Expression of genes associated with DICs (paired t-test) in Normal, CdLS and CHOPs cells. **h.** Binding of Rad21, NIPBL, AFF4, H3K27ac, Pol2 and Pol2ser5 on LC-DICs. Dashed lines represent the average binding signal of each TF on all cohesin sites. Wilcoxon signed-rank test was used to compute *p*-values. **i.**

809 Proposed model for our DICs. Briefly, intragenic loops formed by LC-DICs pause Pol2, whereas
810 HC-DICs form CTCF-mediated loops. Transcription stimulation could displace DICs and disrupt DIC
811 loops, consequently releasing the Pol2 pause. The exposed enhancer sites on LC-DICs then bind their
812 respective TFs and interact with promoters.